Springer

Journal of
Mechanical
Science and
Technology

Journal of Mechanical Science and Technology 23 (2009) 2492~2501

www.springerlink.com/content/1738-494x
DOI 10.1007/s12206-009-0422-4

Parallel computation of two-phase flow in a microchannel using the lattice Boltzmann method †

Suresh Alapati, Sangmo Kang and Yong Kweon Suh*

Department of Mechanical Engineering, Dong-A University, Saha-gu, Busan, 604-714, Korea

(Manuscript Received March 16, 2009; Revised April 2, 2009; Accepted April 2, 2009)

Abstract

We present a numerical simulation of two-phase flow in a three-dimensional cross-junction microchannel by using the lattice Boltzmann method (LBM). At first, we validated our LBM code with the velocity profile in a 3-dimensional rectangular channel. Then, we developed a lattice Boltzmann code based on the free energy model to simulate the immiscible binary fluid flow. The parallelization of the developed code is implemented on a PC cluster using the MPI program. The numerical results of two-phase flow in the microchannel reveal droplet formation process, which compares well with corresponding experimental results. The size of droplet decreases with increase of the flow-rate ratio and the capillary number. The movement of a droplet through the microchannel induces three-dimensional circulating flow inside the droplet. This complex flow is thought to enhance the mixing and reaction of reagents.

Keywords: Free-energy model; Lattice Boltzmann method; Microchannel; Mixing; Two-phase flow

1. Introduction

Microfluidics-based miniaturized systems have been extensively used in the field of chemical and biological applications. The microfluidic devices offer so many advantages due to their miniaturized nature. Since the volume of fluids within these devices is very small, the amount of reagents and analytes used is quite small. Multi-phase flows are very common in microfluidic devices as the surface tension forces are dominant in micro scales [1]. Simulation of multi-phase flows is an interesting and challenging task because of moving and deformable interfaces. In conventional CFD approaches such as finite volume method (FVM) and finite difference method (FDM), we have to track the interface between two phases separately with, e.g., volume of fluid (VOF), level-set method, and front tracking method, etc. The level-set method may break mass conservation for each phase in some cases (particularly when large geometrical change occurs around the interface), and most of the VOF methods suffer from first-order accuracy. Also, these methods are computationally expensive due to interface tracking cost.

Recently, fluid dynamics researchers have paid significant attention to the lattice Boltzmann method (LBM) [2, 3] to simulate complex fluid flows (multiphase flows, flows through porous media, magnetohydrodynamics). Unlike conventional CFD approaches, LBM doesn't solve discretized Navier-Stokes equations. Instead, it solves the Boltzmann kinetic equation on a discrete lattice mesh. The LBM offers the following advantages: (1) It is completely free from solving the Poisson equation (which takes 60-80 % computational time in FVM, FDM techniques), (2) the algorithm is quite simple, which only involves a series of collision and streaming steps, (3) flows involving complex boundaries and interfacial effects can be treated easily, because of its kinetic nature, and (4) it is an ideal candidate for parallel computing as it generally needs only nearest neighbor

† This paper was recommended for publication in revised form by Associate Editor Dongshin Shin

*Corresponding author. Tel.: +82 51 200 7648, Fax.: +82 51 200 7656
E-mail address: yksuh@dau.ac.kr

information (in streaming step). The LBM can be easily applied to microfluidics as complex geometries as well as multiphase flows are involved in these devices. Because of the above advantages, in this study we selected the LBM as a numerical tool for simulating two-phase flow and investigating the droplet formation in a cross-junction microchannel.

To study the influence of various parameters (flow rate, surface tension, and channel geometry) on droplet size and shape, we need to perform extensive experimental works. Numerical simulation of such a system considerably reduces the cost of experimentation. Parallelization of the algorithm is further necessary for carrying out the parametric study of the droplet dynamics.

On the other hand, the challenging problem associated with microfluidic devices is rapid mixing and reaction of reagents. Two streams injected into a microchannel mix only by diffusion mechanism because of low Reynolds number flows. So the length of the channel should be long enough for proper mixing of reagents and the time needed for complete mixing is long. The movement of a droplet through a microchannel develops recirculation flows inside the droplet that enhances mixing [4]. So the droplet-based microfluidics has attracted significant attention. In this paper the internal flow of a droplet is also of our concern.

The paper is organized as follows: The lattice Boltzmann method for simulating two phase flow is explained in Section 2. Validation of LBM code is presented in section 3. Parallel implementation details of our code on a PC cluster are outlined in Section 4. The numerical results obtained from the simulation of two-phase flow in a cross-junction channel are presented in Section 5. Finally, in section 6 conclusions of the present study are drawn.

2. Numerical method

2.1 Lattice Boltzmann scheme

There exist several models to simulate two-phase flows by the lattice Boltzmann approach. In this study we selected the model developed by Orlandini et al. [5] and swift et al. [6], also known as the free-energy model in order to simulate the two-phase flow in a cross-junction microchannel. The advantage of a free energy model is that the equilibrium state of macroscopic properties is thermodynamically consistent [7]. In this method the dynamics of a two phase model is defined by introducing two sets of distribution functions. The density distribution function, $f_i(\mathbf{x},t)$ is used to model the total density (ρ), which recovers Navier-Stokes equations and the order parameter distribution function, $g_i(\mathbf{x},t)$ is used to model the density difference (ϕ), which recovers the convective Cahn–Hilliard equation. The evolution of both distribution functions is governed by the single relaxation time Boltzmann equations reading

$$f_i(\mathbf{x}+\mathbf{c_i}\Delta t, t+\Delta t) - f_i(\mathbf{x},t) = -\frac{1}{\tau}[f_i(\mathbf{x},t) - f_i^{eq}(\mathbf{x},t)], \quad (1)$$

$$g_i(\mathbf{x}+\mathbf{c_i}\Delta t, t+\Delta t) - g_i(\mathbf{x},t) = -\frac{1}{\tau_\phi}[g_i(\mathbf{x},t) - g_i^{eq}(\mathbf{x},t)]. \quad (2)$$

Here $f_i^{eq}(\mathbf{x},t)$ and $g_i^{eq}(\mathbf{x},t)$ are local equilibrium distribution functions defined along the link *i* at each lattice site **x** and each time *t*, τ and τ_ϕ are independent relaxation parameters, and $\mathbf{c_i}$ represents the lattice velocity vectors, defined as $|\mathbf{c_i}| = \Delta x/\Delta t \equiv c$. Here we worked with a cubic lattice consisting of 19 velocity vectors in 3-dimensions [8] (D3Q19 lattice). Fig. 1 shows the D3Q19 lattice.

The distribution functions are related to the total density ρ , fluid momentum $\rho\mathbf{u}$ and to the order parameter ϕ through

$$\rho = \sum_i f_i \ , \quad \rho\mathbf{u} = \sum_i f_i\mathbf{c_i} \ , \quad \phi = \sum_i g_i \ . \quad (3)$$

These equations are locally conserved in any collision process and the local equilibrium distribution functions should also satisfy Eq. (3). To obtain the continuum equations pertinent to a binary fluid mixture, the

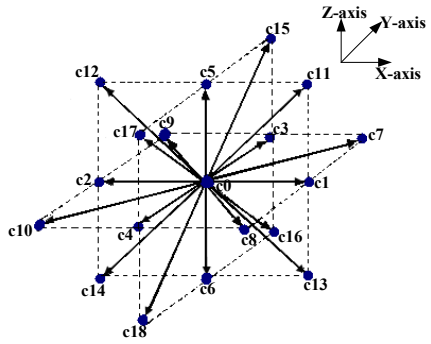

Fig. 1. D3Q19 (3D with 19 velocity vectors) lattice.

higher moments of local equilibrium distribution functions can be defined as follows:

$$\sum_i f_i^{eq} c_{i\alpha} c_{i\beta} = c^2 P_{\alpha\beta} + \rho u_\alpha u_\beta, \tag{4}$$

$$\sum_i g_i^{eq} c_{i\alpha} = \phi u_\alpha, \tag{5}$$

$$\sum_i g_i^{eq} c_{i\alpha} c_{i\beta} = c^2 \Gamma \Delta\mu \delta_{\alpha\beta} + \phi u_\alpha u_\beta. \tag{6}$$

The subscripts α and β denote the components along the *x* and *y* directions, respectively, Γ is a coefficient related to the mobility of the fluid, $\delta_{\alpha\beta}$ is the Kronecker delta, $P_{\alpha\beta}$ is the complete pressure tensor, and $\Delta\mu$ is the chemical potential difference between the two fluids, which is responsible for phase separation. The local equilibrium distribution functions can be expressed as an expansion at the second order in the velocity **u** by

$$\begin{aligned} f_i^{eq} &= A + B u_\alpha c_{i\alpha} + C u^2 + D u_\alpha u_\beta c_{i\alpha} c_{i\beta} + G_{\alpha\beta} c_{i\alpha} c_{i\beta}, \\ g_i^{eq} &= a + b u_\alpha c_{i\alpha} + c u^2 + d u_\alpha u_\beta c_{i\alpha} c_{i\beta}. \end{aligned} \tag{7}$$

The values of *A, B, C, D, G* and *a, b, c, d* are different for each lattice vector and are given in van der Graaf et al. [9].

2.2 Free-energy model

In the free-energy model, a free-energy functional (*F*) is used for describing the dynamics of binary fluid mixtures with interfaces between them. An acceptable choice of the free-energy functional is in the following form [9, 10]:

$$F = \int dV [\frac{1}{3}\rho \ln(\rho) + \frac{a}{2}\phi^2 + \frac{b}{4}\phi^4 + \frac{\kappa}{2}(\nabla\phi)^2]. \tag{8}$$

V is the control volume and κ is a coefficient related to the surface tension and thickness of the interface between two fluids. The functional derivative of Eq. (8) gives the chemical potential difference between the two fluids:

$$\Delta\mu = \frac{\delta F}{\delta \phi} = a\phi + b\phi^3 - \kappa\nabla^2\phi\ . \tag{9}$$

The isotropic (scalar) part p_0, of the pressure tensor ($P_{\alpha\beta}$) specified in Eq. (4) is given by [11]

$$\begin{aligned} p_0 &= \phi\frac{\delta F}{\delta\phi} + \rho\frac{\delta F}{\delta\rho} - \psi(\rho,\phi) \\ &= \frac{1}{3}\rho + \frac{a}{2}\phi^2 + \frac{3b}{4}\phi^4 - \kappa\phi(\nabla^2\phi) - \frac{\kappa}{2}(\nabla\phi)^2. \end{aligned} \tag{10}$$

In this equation, $\psi(\rho,\phi)$ is the free-energy density, which is the integrand of Eq. (8). By ensuring mechanical equilibrium, $\partial_\alpha P_{\alpha\beta} = 0$, we can derive the equation for the pressure tensor ($P_{\alpha\beta}$) [11]:

$$P_{\alpha\beta} = p_0\delta_{\alpha\beta} + \kappa\partial_\alpha\phi\partial_\beta\phi. \tag{11}$$

The first term in the integrand of Eq. (8) is related to the total density (pressure) of fluid and does not affect the phase behavior. The terms having ϕ are related to phase separation. The parameter *b* is always positive, but negative values have to be chosen for the parameter *a,* for immiscible fluids. The equilibrium value of the order parameter in the bulk of two fluids can be obtained with $\phi_0 = \pm\sqrt{-a/b}$. Further, we set $b = -a$ so that the equilibrium values of the order parameter become the predetermined ones ($\phi_0 = \pm 1$). The profile of order parameter at the interface between two immiscible phases (e.g., water and oil) is given by [9]

$$\phi(n) = \phi_0 \tanh\left(\frac{n}{\xi}\right). \tag{12}$$

Here n is the normal co-ordinate to the interface and ξ is the interfacial width, to be calculated from $\xi = \sqrt{2\kappa/a}$. The interfacial tension σ is given by

$$\sigma = \int_{-\infty}^{+\infty} \kappa(\partial_x\phi)^2 dx. \tag{13}$$

By substituting the profile equation, Eq. (12), into Eq. (13) gives the expression for calculating the interfacial tension between two-phases, which is given by

$$\sigma = \frac{4\kappa\phi_0^2}{3\xi}. \tag{14}$$

3. Validation of code

Our numerical code is verified by applying it to the single phase flow in a rectangular channel. Fully developed flow in a long channel with a flat rectangular

cross section, of width $2W$ and height $2H$ (walls at $x=\pm W$ and $z=\pm H$) has a specific flow profile depending on the values of W and H. The general solution for flow in a rectangular cross section channel is given below [12]:

$$v_y(x,z)=\frac{\Delta P W^2}{8\mu}\left[1-\left(\frac{2x}{W}\right)^2+\sum_{n=1}^{\infty}(-1)^n\frac{32}{(2n-1)^3\pi^3}\right]\times\frac{\cosh[(2n-1)\pi z/W]}{\cosh[(2n-1)\pi H/2W]}\cos[(2n-1)\pi x/W], \quad (15)$$

Where $v_y(x,z)$ is velocity in the streamwise direction (y-direction here), μ is the dynamic viscosity, and ΔP is the pressure drop over the channel. We compare the equilibrium velocity profile obtained by LBM with that given by analytical solution (Eq. 15). Fig. 2 shows the variation of velocity in x and z directions, for the aspect ratio of the channel equal to 2. The agreement is almost exact indicating that our numerical code is reliable. After this validation, we developed an LBM code for simulating two-phase flow. The developed lattice Boltzmann code is further parallelized on a PC cluster.

4. Details of the parallel implementation

The PC cluster used for our simulation is a type of Beowulf cluster consisting of one master node (server) and 42 diskless client nodes. Red Hat Linux operating system is installed on the master node. Each client node employs the network booting to load its operating system from the server. The nodes are connected through local network using 48-port, 10/100/1000 GB switch hub. MPI implementation is done by installing LAM/MPI library. The lattice Boltzmann code is developed based on MPI Fortran using SPMD (Single program multiple data) technique. In the SPMD model the computational domain is split into several sub-domains using domain decomposition technique [13], and multiple copies of the same program run simultaneously on each node. Each node computes its own set of data on a sub-domain. At the end of each iteration step, data residing on the boundaries of sub-domain are exchanged with the neighboring nodes using MPI subroutines.

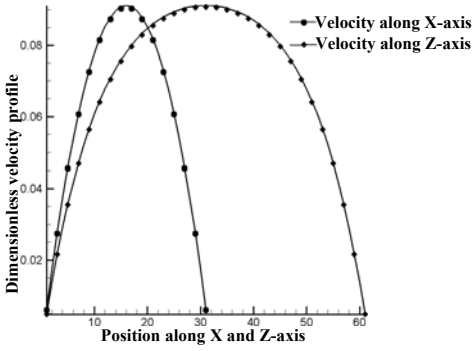

Fig. 2. Comparison of the velocity profile obtained from LBM with the analytical solution. The symbols represent the values from analytical solution given in Eq. (15).

5. Numerical results

5.1 Droplet formation process

To study the dynamics of two-phase flow, the simulations are performed on a standard cross-junction microchannel, which has three inlet ports and one outlet port as shown in Fig. 3. The widths of the main and lateral channels are set at 200μm and 100 μm respectively. The depth of each channel is taken as 100 μm . The simulations are performed on a cubic lattice of size $17\times391\times238$ in x, y and z directions, respectively. The computational domain is split into 29 sub-domains for parallel processing. Fluid A phase with flow rate Q_A is admitted through the main-channel inlet, while Fluid B phase is admitted through each entrance of two lateral channels with the flow rate Q_B. No-slip boundary condition is applied for all the solid walls of the channel by the second-order mid-plane bounce back scheme [10]. The boundary conditions at the three inlets are also treated by using the bounce-back scheme. Uniform velocity profiles are given at the inlets of fluid A and fluid B.

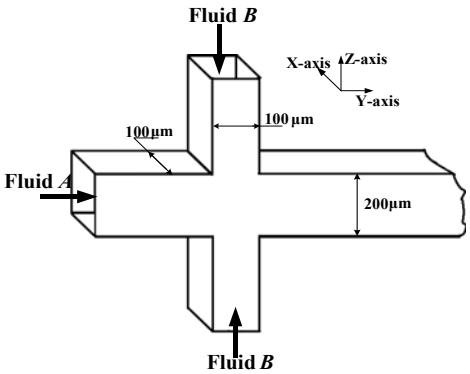

Fig. 3. 3D cross-junction microchannel considered in simulation.

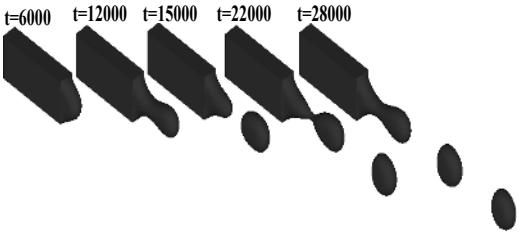

Fig. 4. Snap shots of the droplet formation in a cross-junction microchannel at different time steps.

At the outlet, Neumann boundary condition is applied. To allow slippery transport of the droplets (fluid A here) without sticking to the channel walls, the carrier fluid (fluid B here) must wet the walls of the microchannel [14]. If this condition is met, the droplets do not come in contact with the walls and remain separated from the wall by thin layer of carrier fluid. So, in our simulation the order parameter value at walls is set to be equal to -1.0, which is the same value of the fluid B. The contour of the order parameter value is used to depict the 3D interface.

Fig. 4 shows the isosurfaces of the order parameter value at different time steps, which reveals the droplet formation process. The side channels are not shown in this figure. The fluid phases (fluid *A* and fluid *B*), which are injected from 3 inlets intersect at the cross-junction, and the fluid *A* is compressed by shear force due to the interfacial tension between two fluids and cut-off into droplets of finite size. The droplets are frequently generated at the cross-junction and travel downstream through the channel.

Fig. 5 shows the detailed process of droplet formation and corresponding velocity vectors at the central yz-plane. The numerical results are compared with the available experimental results [15]. The ratio of flow rates between two fluids (Q_B/Q_A) is kept at 3, following the experimental set-up. In the simulation, we set kinematic viscosity $\nu = 4.4 \times 10^{-06} m^2/s$, interfacial tension between two fluids, $\sigma = 0.015\ N/m$ and velocity of fluid *A*, V_A=0.002 m/s. From Fig. 5 it can be noticed that the agreement is satisfactory in the droplet formation process and in the velocity field, which proves that our simulation can be successfully applied to two-phase flow in a microchannel. Fig. 5 also gives the comparison of present 3D results with 2D results obtained by Li et al [10]. From this comparison we can say that the 3D simulation of droplet formation gives better agreement with experimental results than 2D simulation.

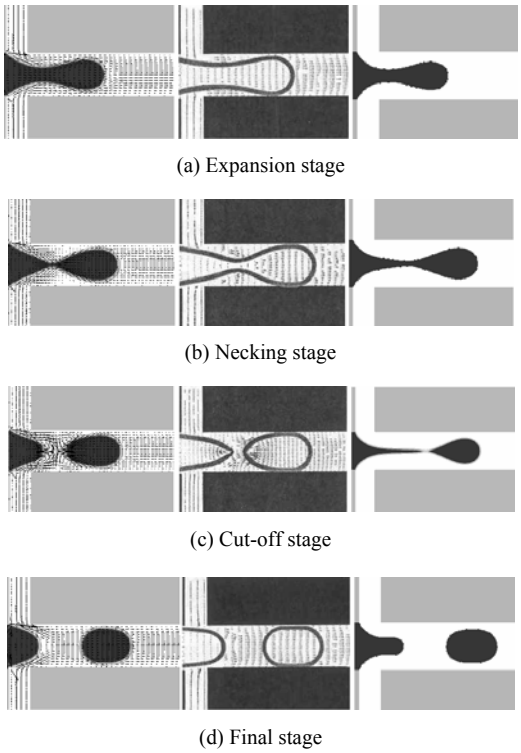

(a) Expansion stage

(b) Necking stage

(c) Cut-off stage

(d) Final stage

Fig. 5. Different stages of droplet formation process in a cross-junction Microchannel. Left side part of the figure represents 3-D numerical results, middle one represents experimental results, and right side part represents 2-D results.

Fig. 5 depicts four stages of the droplet formation process. The advancement of fluid *A* in the expansion stage, Fig. 5(a), takes place slowly and steadily. The necking stage, Fig. 5(b), illustrates that the fluid *A* is compressed by the fluid *B* from the two sides. At this stage the fluid *A* is about to split from the bulk phase. The interfacial tension forces increase here and become strong due to the sudden change in the curvature of the interface. Fig. 5(c) shows the cut-off stage in which fluid *A* is suddenly cut-off from the bulk and a droplet is generated. After cut-off, four symmetric vortices appear on the back of the generated droplet. These vortices should enhance the mixing and chemical reaction. In the final stage shown in Fig. 5(d), the generated droplet tends to minimize its surface area and attains a particular shape. The competition between interfacial tension and imposed pressure gradient at the interface resulted in droplets of a finite diameter. The shape and size of each droplet depends on the flow-rate ratio between two fluids. In the present study, droplet formation as a function of flow rate and capillary number is simulated.

5.2 Effect of the flow rate of fluid B

Fig. 6 shows the droplet size and shape of droplets generated as a function of continuous phase (fluid *B*) flow rate, while the dispersed phase (fluid *A*) flow rate is kept constant at 4.8 $\mu L/\min$. From Fig. 6, we infer that slugs (slug means a droplet of rectangular shape, in which the droplet length is more than the channel height) are formed when the flow rate is low, and the shape becomes more circular as the flow rate increases. The droplet size also decreases when the flow rate increases.

The graphical representation of the droplet size and distance between two successive droplets as a function of fluid *B* flow rate (Q_B) is shown in Fig. 7. The distance between droplets increases when Q_B increases, because the velocity of a droplet also increases with the increase in flow rate of fluid *B* (refer to Table 1 for the velocity of droplet at different values of Q_B). This indicates that the droplets are transported to the down stream with the same velocity as that of carrier fluid. We can relate the flow rate of fluid *A* to the droplet volume by

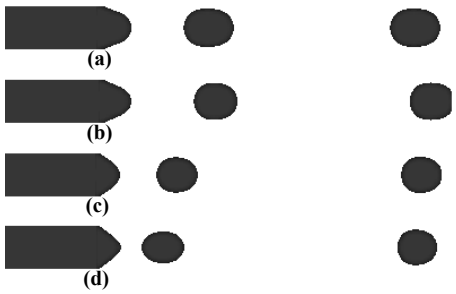

Fig. 6. Droplet size and shape as a function of continuous phase flow rate. (a) Q_B=9.6 $\mu L/\min$, (b) Q_B=14.4 $\mu L/\min$, (c) Q_B=19.2 $\mu L/\min$, (d) Q_B=24 $\mu L/\min$.

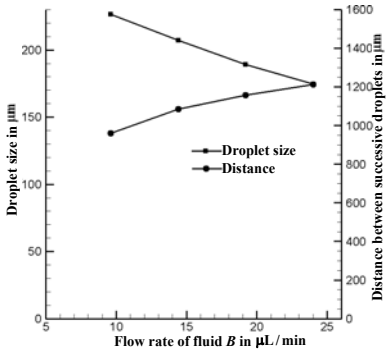

Fig. 7. Droplet size and distance between droplets as a function of Q_B.

$$Q_A = \frac{V_d}{T_p}. \tag{16}$$

Here V_d is volume of the droplet generated and T_p is the time period between two successive droplets. T_p can be written as the ratio of distance (L_p) between two successive droplets to the droplet velocity (U_d). So finally the flow rate Q_A is formulated by

$$Q_A = \frac{V_d U_d}{L_p}. \tag{17}$$

We calculated the flow rate of fluid *A* from Eq. (17) and compared it with the actual flow rate. The volume of the droplet (V_d) in Eq. (17) is calculated from the cross-sectional area and the droplet length measured along the center line of the channel. The cross-sectional area is evaluated by assuming approximate shape (slug, elliptical, or circular) for the droplet. Table 1 gives the comparison of actual flow rate Q_A with calculated one, the approximate shape of droplet for different values of flow-rate ratio (Q_B/Q_A). In Table 1, the calculated values of flow rates are slightly higher than the actual ones. The reasons for this deviation are, first, the shape of droplet for calculating the volume is approximated, and second, the curvature effect at the corners and sides of the droplet is completely ignored.

5.3 Effect of the flow rate of fluid A

Fig. 8 shows the droplet size and shape of droplets generated as a function of Q_A, while Q_B is kept constant at 18 $\mu L/\min$. From Fig. 8, we can deduce that the droplet size increases with Q_A. By observing Fig. 6 and Fig. 8 we can presume that the size and shape of droplets are almost the same for the same flow-rate ratio between two phases, Q_B/Q_A. So the droplet size mainly depends on the ratio of flow rate, and it decreases with the increase of the ratio.

Table 1. Comparison of actual flow rate Q_A with that calculated from Eq. (17).

Q_A ($\mu L/\min$)		Ratio of Q_B/Q_A	U_d (mm/s)	Approx. shape of droplet
Actual	Calculated			
4.8	5.32	2	27.5	Rectangular
4.8	5.5	3	36.5	Elliptical
4.8	6.30	4	46.5	Circular
4.8	6.93	5	60	Circular

Table 2. Comparison of actual flow rate of fluid A (Q_A) with that calculated from eq. (17).

Q_A (μL / min)		Ratio of Q_B/Q_A	U_d (mm/s)	Approx. shape of droplet
Actual	Calculated			
9	11.8	2	50	Rectangular
6	8.1	3	47	Elliptical
4.5	6.0	4	45	Circular
3.6	4.13	5	42.5	Circular

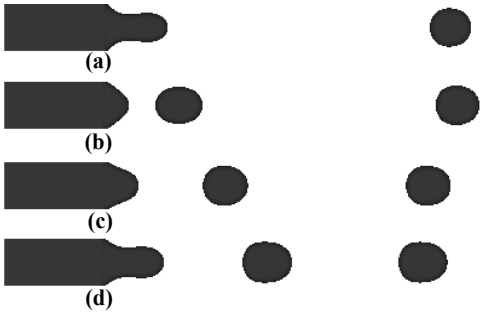

Fig. 8. Droplet size and shape as function of dispersed phase flow rate. (a) Q_A=3.6 μL / min , (b) Q_A=4.5 μL / min , (c) Q_A=6 μL / min , (d) Q_A=9 μL / min .

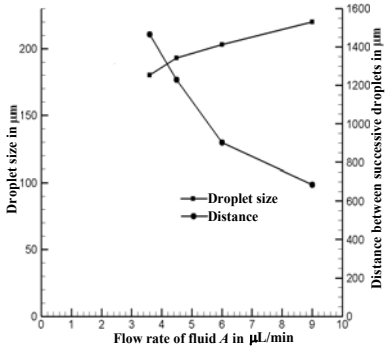

Fig. 9. Droplet size and distance between droplets as a function of Q_A.

Fig. 9 depicts the graphical representation of the droplet size and distance between two successive droplets as a function of Q_A. The distance between droplets decreases when Q_A increases. But the variation of distance between droplets with Q_A is more pronounced than that with Q_B (from Figs. 6-9), for the same flow-rate ratio (Q_B/Q_A). This is because the velocity of droplet is almost constant as Q_B is kept constant in this case (refer to Table 2 for the velocity of droplet at different values of Q_A). In this case too we calculated the flow rate of fluid A from droplet parameters using Eq. (17), the result being shown in

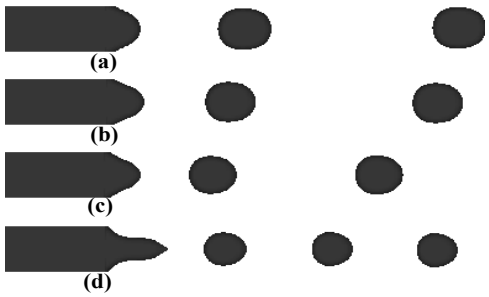

Fig. 10. Droplet size variation as a function of capillary number. (a) Ca=0.00115 (b) Ca=0.0016, (c) Ca=0.0023, (d) Ca=0.0047.

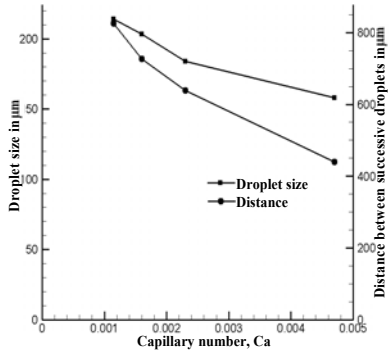

Fig. 11. Droplet size and distance between droplets as function of capillary number.

Table 2. From Tables 1 and 2, we can see that the droplet shape is the same for the same flow-rate ratio (Q_B/Q_A).

5.4 Effect of the capillary number

Simulation of the droplet formation for different values of capillary numbers is also carried out. The capillary number based on the droplet velocity is defined as,

$$Ca = \frac{\mu U_d}{\sigma}. \tag{18}$$

The simulations are carried out by changing the interfacial tension value, by keeping all the other variables constant. Fig. 10 represents the droplet formation as a function of the capillary number. The droplet size decreases when the capillary number increases.

The graphical representation of the droplet size and distance between two successive droplets as a function of capillary number is shown in Fig. 11. The distance between droplets decreases with an increase of the capillary number. This is because the droplet

size decreases with increase of the capillary number, and the velocity of droplet is same as the flow rate is kept constant. In all the above results the flow continuity is satisfied, which proves our code can be successfully applied to the droplet formation process at various flow rates and interfacial tensions.

5.5 Internal flow of a moving droplet

The movement of a droplet through a straight microchannel gives rise to flow inside the droplet. The internal flow of a droplet is presented in terms of the coordinates moving with the same velocity as the droplet. Fig. 12 shows the internal flow at different planes of a droplet. Each plane encompasses the center of the droplet. The white region in Fig. 12 represents the droplet and the dark the carrier fluid. The walls of the microchannel are denoted by shaded area. The droplet is moving to the *y*-direction; the width and height of droplet are in *x* and *z*-directions, respectively.

From Fig. 12(b) we notice that the droplet contacts the four sides of the microchannel, while moving. The droplet is dragged by microchannel walls and a backward flow is generated at these contact surfaces (Fig. 12(a), (c)). The amount of dragging is proportional to the contact area of the droplet. This contact area is larger at the side walls than at the top and bottom walls of the microchannel (see Fig. 12(b)). So the amount of backward flow is more in the XY-plane than in the YZ-plane. On the other hand, the droplet does not contact the walls at the four corners due to its round shape. This round shape forms gaps at the four corners, and these gaps are filled with carrier fluid phase (see Fig. 12(b)). The liquid-liquid interface slips freely at these four corners of the microchannel. The liquid-liquid interfaces near the corners generate the forward flow. The fluid which is dragged by walls in backward direction must return forward within the droplet to satisfy the continuity equation. Combination of the backward flow at walls and the forward flow at corners enforces the fluid to circulate within the droplet. As observed from Fig. 12(a), the fluid at the walls flows backwards and the fluid at the centre forward. This flow pattern generates a pair of symmetrical vortices. A similar flow pattern is observed in the XY-plane. But the backward flow is stronger in the XY-plane due to a large contact area with the walls. These vortices in different planes generate complex circulation flows in a closed volume of the droplet. These 3-dimensional vortices should play an important role for enhancement of the mixing and chemical reaction inside the droplet.

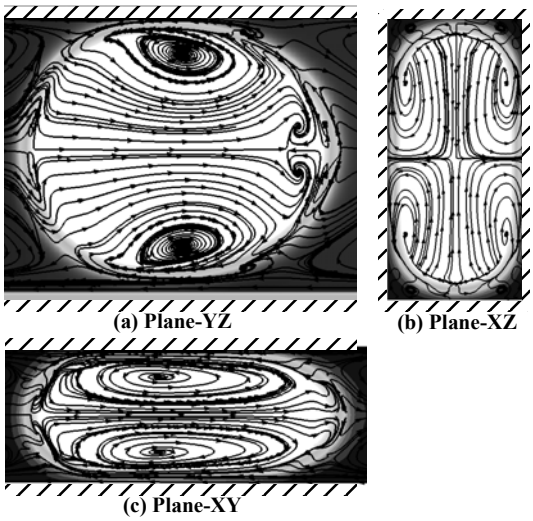

Fig. 12. Internal flow of a moving droplet at different planes.

6. Conclusions

Simulation of two-phase flow inside a cross- junction microchannel has been carried out successfully using the lattice Boltzmann method (LBM) with a parallel programming technique. Due to the pressure and interfacial-tension effect, the dispersed phase which is injected from the main inlet of the microchannel is cut into droplets periodically by the continuous phase which is injected from the other inlets. The numerical results compared well with the available experimental visualization results, which proves the ability of our code in simulation of two-phase flows. Further it was shown that our 3-D numerical results give better agreement with experimental ones than 2-D simulation. After performing the droplet formation simulations with different flow rates and capillary numbers, we conclude that the droplet size and shape mainly depend on flow-rate ratio (Q_B/Q_A) and interfacial tension between two phases. When a droplet moves through the microchannel, the drag force on the droplet contact surfaces with the microchannel walls causes the fluid inside the droplet to circulate with complex three-dimensional pattern in a closed volume. This circulation flow enhances mixing and chemical reaction.

Acknowledgment

This work was supported by the Korea Science and Engineering Foundation (KOSEF) through National Research Laboratory Program funded by Ministry of Science and Technology (No. 2005-01091).

References

[1] C. N. Baroud and H. Willaime, Multiphase flows in microfluidics, *C. R. Physique*, 5(5) (2004) 547-555.

[2] R. Benzi, S. Succi and M. Vergassola, The lattice Boltzmann equation: theory and applications, *Phys. Rep*., 222 (3) (1992) 145-197.

[3] S. Succi, *The Lattice Boltzmann Equation for Fluid Dynamics and Beyond*, Oxford University press, Oxford, UK, (2001).

[4] H. Kinoshita, S. Kaneda, T. Fujii and M. Oshima, Three-dimensional measurement and visualization of internal flow of a moving droplet using confocal micro-PIV, *Lab Chip,* 7 (3) (2007) 338-346.

[5] E. Orlandini, M. R. Swift and J. M. Yeomans, A lattice Boltzmann model of binary-fluid mixtures, *Europhys. Lett.,* 32 (6) (1995) 463-468.

[6] M. R. Swift, E. Orlandini, W. R. Osborn and J. M. Yeomans, Lattice Boltzmann simulations of liquid-gas and binary fluid systems, *Phys. Rev. E,* 54 (5) (1996) 5041-5052.

[7] M. R. Swift, E. Orlandini and J. M. Yeomans, Lattice Boltzmann simulation of nonideal fluids, *Phys. Rev. Lett.*, 75 (5) (1995) 830-833.

[8] Dieter A. Wolf-Gladrow, *Lattice-Gas Cellular Automata and Lattice Boltzmann Model,* Springer, Germany, (2000).

[9] S. van der Graaf, T. Nisisako, C. G. P. H. Schroën, R. G. M. van der Sman and R. M. Boom, Lattice Boltzmann simulations of droplet formation in a T-shaped microchannel, *Langmuir,* 22 (9) (2006) 4144-4152.

[10] Z. Li, J. Kang, J. H. Park and Y. K. Suh, Numerical simulation in a cross-junction microchannel using the lattice Boltzmann method, *J. Mech. Sci. & Tech.*, 21 (1) (2007) 162-173.

[11] A. Xu, G. Gonnella and A. Lamura, Phase-separating binary fluids under oscillatory shear, *Phys. Rev. E,* 67 (5) (2003) 056105(0-14).

[12] P. Gondret, N. Rakotomalala, M. Rabaud, D. Salin and P. Watzky, Viscous parallel flows in finite aspect ratio Hele-Shaw cell: Analytical and numerical results, *Phys. Fluids,* 9 (6) (1997) 1841-1843.

[13] C. Körner, T. Pohl, U. Rüde, N. Thürey and T. Zeiser, Parallel Lattice Boltzmann Methods for CFD Applications, Book chapter in *Numerical Solution of Partial Differential Equations on Parallel Computers,* Springer, Germany, 51 (2006) 439-466.

[14] J. D. Tice, H. Song, A. D. Lyon and R. F. Ismagilov, Formation of Droplets and Mixing in Multiphase Microfluidics at Low Values of the Reynolds and the Capillary Numbers, *Langmuir,* 19 (22) (2003) 9127-9133.

[15] K. C. Kim, J. M. Kim and S. Y. Yoon, Simultaneous measurement of internal and external flow fields around the droplet formation in a microchannel, *proc. Of 4th KSV Conf.,* Korea, (2004) 80-83.

Suresh Alapati received his B.Tech. degree in Mechanical Engineering from Acharya Nagarjuna University, India, in 2004. He then received his M. Tech. degree from NIT, Calicut, India in 2006. Mr. Suresh is currently a Ph.D. student at the Department of Mechanical Engineering at Dong-A University in Busan, Korea. His research interests are simulation of micro/nano biological flows and mixing in microfluidic devices.

Sangmo Kang received B.S. and M.S. degrees from Seoul National University in 1985 and 1987, respectively, and then worked for five years in Daewoo Heavy Industries as a field engineer. He also achieved a Ph.D. in Mechanical Engineering from the University of Michigan in 1996. Dr. Kang is currently a Professor at the Division of Mechanical Engineering at Dong-A University in Busan, Korea. Dr. Kang's research interests are in the area of micro- and nanofluidics and turbulent flow combined with the computational fluid dynamics.

Yong Kweon Suh received his B.S. in Mechanical Engineering from Seoul National University, Korea, in 1974. He then received his M.S. and Ph.D. degrees from SUNY Buffalo in 1985 and 1986, respectively. Dr. Suh is currently Professor at the Department of Mechanical Engineering at Dong-A University in Busan, Korea. His research interests include electrokinetic phenomena such as electro-osmosis, electrophoresis, motion of magnetic particles, and mixing in micro/nano scales.